Celest Mech Dyn Astr (2012) 112:253–282
DOI 10.1007/s10569-011-9396-5

ORIGINAL ARTICLE

Unified State Model theory and application in Astrodynamics

V. Vittaldev · E. Mooij · M. C. Naeije

Received: 19 April 2011 / Revised: 15 December 2011 / Accepted: 23 December 2011 /
Published online: 3 February 2012

Abstract The Unified State Model is a method for expressing orbits using a set of seven elements. The elements consist of a quaternion and three parameters based on the velocity hodograph. A complete derivation of the original model is given in addition to two proposed modifications. Both modifications reduce the number of state elements from seven to six by replacing the quaternion with either modified Rodrigues parameters or the Exponential Map. Numerical simulations comparing the original Unified State Model, the Unified State Model with modified Rodrigues parameters, and the Unified State Model with Exponential Map, with the traditional Cartesian coordinates have been carried out. The Unified State Model and its derivatives outperform the Cartesian coordinates for all orbit cases in terms of accuracy and computational speed, except for highly eccentric perturbed orbits. The performance of the Unified State Model is exceptionally better for the case of orbits with continuous low-thrust propulsion with CPU simulation time being an order of magnitude lower than for the simulation using Cartesian coordinates. This makes the Unified State Model an excellent state propagator for mission optimizations.

Keywords Unified State Model · Quaternion · Modified Rodrigues parameters · Orbit propagation · Exponential map · Hodograph

1 Introduction

Cartesian coordinates and classic Keplerian elements are well-established for the propagation and visualization of orbits. However, there are many other methods in which satellite orbits can be described. One of these is the Unified State Model (USM). The USM, first proposed by Altman (1972), uses quaternions and velocity-hodograph parameters to express orbits.

V. Vittaldev · E. Mooij (✉) · M. C. Naeije
Faculty of Aerospace Engineering, Delft University of Technology, Building 62, Kluyverweg 1, 2629 HS Delft, The Netherlands
e-mail: E.Mooij@TUDelft.nl

The four quaternion elements express the orientation of a reference frame fixed to the orbiting body, with respect to an inertial frame fixed to the central body. The velocity hodograph parameters give information about the size and shape of the orbit. During an unperturbed orbit, the velocity hodograph parameters remain constant and only the quaternion varies with time. This is because the orbital shape remains unchanged for such an orbit, and only the location of the orbiting body within the orbit changes with time. When perturbations are present, the variation of the hodographic parameters will be small compared to the variation of Cartesian coordinates. Consequently, the USM will have better numerical stability than Cartesian coordinates as it has four relatively fast varying and three slowly varying elements, in contrast with six rapidly varying elements. The period of the variation of the Cartesian coordinates is equal to one orbital period. The four relatively fast varying USM elements have a period equal to two orbital periods. The classic Keplerian elements have only one rapidly varying element, which is the true anomaly. However, singularities exist and the equations for the influence of perturbations are rather complex. There are also other interesting singularity-free orbit element sets such as the Modified Equinoctial Elements (Hintz 2008). However, these also have quite complex dynamics and beyond the scope of this work. Quaternions have also been used in conjunction with orbital mechanics in other literature. A simplification of the three-dimensional Kepler problem into a perturbed harmonic oscillator can be found in Waldvogel (2006). An extension of the aforementioned technique that allows for efficient integration of close encounters in the two-body perturbed problem can be found in Fukushima (2007a,b). There are also accurate techniques that combine variation of parameters with quaternions (Pelaez et al. 2007). And, models exist that combine the Kustaanheimo-Steifel regularizing transformation with quaternions for orbital motion (Vivarelli 1983, 1985).

The USM, which can be used for numerical integration of perturbed orbits, is intended to be a competitor to the standard Cowell's method of integration. This is useful for quick first-order mission-analysis problems. However, for very accurate integration of orbits, more analytically complex integration methods can be used. These include using the Kustaanheimo–Steifel transform (Kurcheeva 1977; Yoshida 1982) and the Sperling–Burdet transform (Silver 1975; Jezewski 1975). Furthermore, so-called symplectic integrators exist that conserve the two-form of the Hamiltonian of the dynamic system (Breiter 1998; Petit 1998; Tsitouras 1999). It should be stressed that the USM is not intended to compete with these high-accuracy methods.

Not much research on the USM has been carried out since 1972. If the theory is mentioned, it has always been in relation to navigation. A method of satellite tracking in velocity space rather than the traditional position space was shown in Altman (1975), which has been mentioned in Raol and Sinha (1985) but never investigated further. The USM equations have been shown in more detail in Chodas (1981), but with a term differing from the original model found in Altman (1972). These modified equations are also shown in Raol and Sinha (1985). Both Raol and Sinha (1985) and Chodas (1981) focus on satellite orbit tracking and mention that the USM allows for better trajectory simulation. It was concluded by Chodas (1981) that satellite orbit tracking from a ground station is slightly better using the traditional Cartesian coordinates than with the USM. Therefore, the strategy in Raol and Sinha (1985) is to use the USM for trajectory propagation, and the Cartesian coordinates for state estimation.

As mentioned, the equations of the USM dynamics found in Raol and Sinha (1985), and Chodas (1981) differ from the equations found in Altman (1972). The explanation of the USM in Chodas (1981) contains more detail on the implementation than Altman (1972). It is, however, not easily publicly available and it does not provide a rigorous derivation of the given equations. Since there are two sets of equations provided in three papers, we have

decided to provide a comprehensive derivation of the equations of the USM to discern the correct method. As will be shown in the paper, the equations found in Chodas (1981), and Raol and Sinha (1985) are correct because the full effect of out-of-orbital-plane perturbing accelerations is not present in Altman (1972). It is stated in Altman (1972), Chodas (1981), Raol and Sinha (1985) without any proof that the USM is better for numerical integration than Cartesian coordinates. This statement has only recently been validated by Vittaldev et al. (2010).

There are some methods found in Chodas (1981) that reduce the number of state elements from seven to six. Reducing the number of state elements can result in a smaller computational load, but this is, of course, dependent on the computational load of the underlying dynamics. The main advantage, as stated in Chodas (1981), is the reduction of the computational load for navigation applications. The state transition matrix of an Extended Kalman Filter (EKF) then has 13 fewer elements, and the unscented transformation of the dynamics of a standard Unscented Kalman Filter (UKF) requires two fewer function evaluations. Therefore, one novel method that we propose, the USM6, is to reduce the number of elements by using modified Rodrigues parameters (MRP) instead of a quaternion to express the orientation of the orbital frame. The other method, the USMEM, is to replace the quaternion using an exponential map of the quaternion. The traditional USM is from now on referred to as the USM7 and the common theory is referred to as the USM. Recently, MRP have started to gain popularity, especially for satellite attitude determination and control. MRP can be used in the same way as quaternions to express orientations of coordinate frames, but with three elements instead of four. Although this means that there will be a singularity encountered for certain rotations, this can be effectively bypassed by the use of a shadow set of parameters as can be seen in Sect. 2. Exponential mapping has been mostly used in rigid body simulations for robotics as it can contain the same information as a quaternion but without requiring explicit constraints for Jacobians, without requiring normalizing after integration steps, and having fewer parameters (Grassia 1998).

The main goal of this paper is to make the USM more accessible to researchers and engineers so that the USM can once again be used and hopefully be made generally known. This is done by providing a detailed derivation and by numerically integrating various orbital trajectories to compare the performance of the USM with respect to the standard Cartesian coordinates. The background material required to understand the theory for the USM is presented in Sect. 2. USM combines many concepts that are commonly found in Astrodynamics such as hodographs and in other fields of dynamics such as quaternions, MRP, and exponential maps. However, it is unusual to find them combined in Astrodynamics and therefore, an overview of these concepts is given for the sake of completeness. Section 3 contains the derivation of the classical USM, Sect. 4 presents the modification of USM using MRP and exponential maps, whereas Sect. 5 shows the results of some orbital simulations. Section 6, finally, concludes the paper.

2 Background theory for the USM

In this section, a brief overview of the background information necessary for the derivation and the application of the USM is presented. The traditional USM7 uses quaternions and the velocity hodograph, the USM6 uses MRP instead of a quaternion, and the USMEM uses the exponential map instead of a quaternion. Thus, these three concepts and the rigid-body rotations are introduced here. Hodographs are treated in more detail than rotations because rotations are dealt with in many publications.

2.1 Describing rotations

Reference frames are required to express the position and motion of bodies. Normally, these reference frames are dextral orthonormal triads, meaning that the first axis can be mapped onto the second axis by a 90° right-handed positive rotation along the third axis. Thus, a reference frame $\mathcal{F}_a$ consists of a set of three right-handed, mutually perpendicular vectors: $\hat{\mathbf{a}}_1$, $\hat{\mathbf{a}}_2$, and $\hat{\mathbf{a}}_3$. It is often necessary to use different reference frames within the same set of calculations. In this case, it is required to convert a set of coordinates of a vector expressed in one reference frame to another. This can be done in many different ways. A few that are used in this work are: the direction cosine matrix, Euler axis and angle, quaternions, and modified Rodrigues parameters. Only a cursory overview of rotations and attitude parameters will be presented in this section. For a more thorough explanation, the reader is referred to Hughes (1986) and Schaub and Junkins (2002).

The transformation between two reference frames can be carried out using the so-called direction cosine matrix (DCM). The elements of this matrix are the cosines of the angles between the unit vectors of the two reference frames. The DCM is assumed to be a passive transformation and the notation used is from Hughes (1986). The frame transformation is carried out by pre-multiplying the vector defined in $\mathcal{F}_a$ with the DCM $\mathbf{C}_{b,a}$. To convert a vector from $\mathcal{F}_b$ to $\mathcal{F}_a$, the inverse of $\mathbf{C}_{b,a}$, $\mathbf{C}_{a,b}$, should be used. As $\mathbf{C}_{b,a}$ is an orthonormal matrix, its inverse is simply the transpose. It should be noted that by converting a vector from one frame to another, only the coordinates of the vector are changed, but the vector itself remains untouched.

Another fundamental concept in rotations of reference frames is Euler's theorem (Hughes 1986). This theorem states that any rotation between two frames can be expressed by a rotation of an angle, Φ, around an axis $\hat{\mathbf{a}}$, through the shared origin of the two reference frames. This axis and angle are often referred to as the Euler axis $\hat{\mathbf{a}} = [a_1, a_2, a_3]^T$ and the Euler angle Φ, respectively.

2.1.1 Quaternions

Attitude is synonymous with orientation and in the aerospace world it almost always means the orientation of a spacecraft or an aircraft. The attitude of a spacecraft relative to a reference frame actually means the orientation of a reference frame fixed to the body of the spacecraft with respect to another reference frame. Attitude parameters are just parameters that can describe this orientation. Thus, the DCM, Euler axis and Euler angle are all attitude parameters. Yet another representation, a quaternion, is a 4-dimensional hyper-complex number consisting of one real and three imaginary numbers. Quaternions of unit magnitude are used to express rotations, with the imaginary part being a vector, $\boldsymbol{\epsilon}$, and the real part a scalar, η. The quaternion can be created using the Euler axis-angle in the following manner:

$$\begin{aligned} \boldsymbol{\epsilon} &= \left[\, \epsilon_1,\ \epsilon_2,\ \epsilon_3 \,\right]^T = \hat{\mathbf{a}} \sin(\Phi/2) \\ \eta &= \cos(\Phi/2) \end{aligned} \tag{1}$$

2.1.2 Modified Rodrigues parameters (MRP)

MRP are a modification of the classical Rodrigues parameters, which are stereographic projections of the 4-dimensional unit quaternion sphere onto a 3-dimensional hyperplane using a projection point. This technique is sometimes used to project the 3-dimensional sphere of the Earth onto a 2-dimensional map. An MRP vector $\boldsymbol{\sigma}$, can also be used to

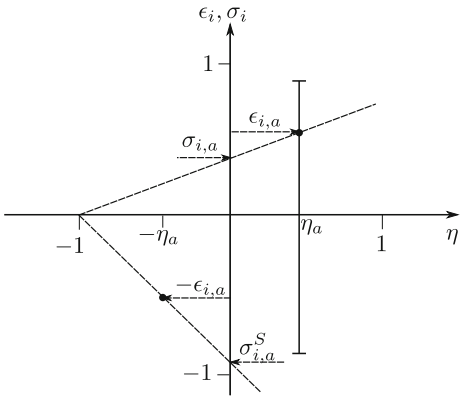

Fig. 1 Stereographic projection of an arbitrary ϵ_i

describe the attitude of a reference frame, and one of their primary uses is in spacecraft attitude determination and control (Jizheng et al. 2008; Crassidis and Markley 1996). The main reason is that a quaternion uses four parameters to represent three degrees of freedom. Therefore, the covariance matrix used to represent the uncertainty of the estimated attitude is prone to become singular. The benefit of using MRP is that only three parameters are required to describe a rotation. However, a singularity exists that can be evaded as will be explained further on.

Since the four quaternion elements lie in four different dimensions, a cross section can be taken of any two dimensions since they are all orthogonal. To view the stereographic projection of any one element of $\boldsymbol{\epsilon}$, $\epsilon_{i=1,2,3}$, the $\epsilon_{i=1,2,3} - \eta$ plane can be viewed as illustrated in Fig. 1. In this 2-dimensional plane, the hyperplane at $\eta = 0$ is the ϵ_i-axis.

An MRP vector can be written in terms of the Euler axis-angle pair as

$$\boldsymbol{\sigma} = \hat{\mathbf{a}} \tan(\Phi/4) \tag{2}$$

From Eq. (2) it can be seen that there is a singularity when the Euler angle is $\pm 360°$. MRP are very closely related to quaternions and are extracted from a DCM by first extracting the quaternion and then converting the quaternion to MRP. For the MRP, the projection point for the stereographic projection is $\left[\boldsymbol{\epsilon}^T,\ \eta\right] = \left[0,\ 0,\ 0,\ -1\right]$. The tangent hyperplane is at $\eta = 0$ and normal to the η-axis. All the rotations can be expressed with a 3-dimensional vector, except for a rotation with $\eta = -1$. This occurs at $\Phi = \pm 360°$.

To avoid the singularity, an alternative set of parameters known as the shadow modified Rodrigues parameters (SMRP), $\boldsymbol{\sigma}^S$, is defined. The property of quaternions that the orientation expressed by $(\boldsymbol{\epsilon}, \eta)$ is the same as the orientation expressed by $(-\boldsymbol{\epsilon}, -\eta)$ is used. Thus, the SMRP vector is a stereographic projection of $(-\boldsymbol{\epsilon}, -\eta)$. The SMRP vector has a singularity at $\eta = 1$. Thus, switching between the MRP and the SMRP avoids encountering this singularity. An MRP vector can be converted to SMRP in the following manner

$$\boldsymbol{\sigma}^S = -\boldsymbol{\sigma}/(\sigma^2) \tag{3}$$

with σ being the norm of $\boldsymbol{\sigma}$. The same procedure is used to convert an SMRP vector to MRP. It should be noted that the conversion is best carried out when $|\boldsymbol{\sigma}|$, or $\left|\boldsymbol{\sigma}^S\right|$ is 1. At this point the MRP vector is the same as the SMRP vector.

2.1.3 Exponential mapping

The Euler axis-angle normally consists of four parameters. Three parameters make up the unit Euler-axis vector and the fourth parameter is the Euler angle. These four parameters can be compressed into a three parameter vector, which is the equivalent of the unit Euler-axis having the magnitude of the Euler angle. The three-parameter set can also be defined as an exponential mapping of quaternions, as found in Grassia (1998). Since the unit Euler-axis is defined as $\hat{\mathbf{a}}$ and the Euler angle as Φ, the exponential map can be defined as $\mathbf{a}$, where

$$\mathbf{a} = \Phi\hat{\mathbf{a}} \tag{4}$$

The EM can be extracted from quaternions in the following way

$$\begin{aligned} \Phi &= 2\arccos\eta \\ \hat{\mathbf{a}} &= \frac{\boldsymbol{\epsilon}}{\sin\Phi/2} \end{aligned} \tag{5}$$

The quaternion parameters can then be extracted from the EM as found in Eq. (1), which can also be written in the following form

$$\begin{bmatrix} \boldsymbol{\epsilon} \\ \eta \end{bmatrix} = \begin{bmatrix} \frac{\sin\Phi/2}{\Phi}\mathbf{a} \\ \cos\Phi/2 \end{bmatrix} \tag{6}$$

In Eq. (6), it can be seen that a singularity exists when $\Phi = 0$. According to Grassia (1998), this singularity can be avoided by using the first two terms of the Taylor series expansion of $\frac{\sin\Phi/2}{\Phi}$, for a sufficiently small value of Φ. If `eps` is defined as the machine precision value, the following approximation is accurate to machine precision when $\Phi \leq \sqrt[4]{\texttt{eps}}$. The first two terms of the Taylor series expansion are then

$$\frac{\sin\Phi/2}{\Phi} \approx \frac{1}{2} + \frac{\Phi^2}{48} \tag{7}$$

The EM parameter set is not singularity free, but has a singularity at integer multiples of 360° like the MRP. Also like the MRP, this singularity can be bypassed by switching to an alternate shadow EM (SEM) set that expresses the same orientation. This is because a rotation expressed by Φ about $\hat{\mathbf{a}}$ is the same as the rotation over $2\pi - \Phi$ about $-\hat{\mathbf{a}}$. Thus, the shadow parameter set $\mathbf{a}^S$ can be extracted from $\mathbf{a}$ in the following manner

$$\mathbf{a}^S = \left(1 - \frac{2\pi}{\|\mathbf{a}\|}\right)\mathbf{a} \tag{8}$$

It should be noted that unlike the MRP, there is no need to keep track of the type of EM used, because the conversion to quaternions is the same for either case. The only need to keep track of the type of EM is if it is desired to carry out interpolation between sets of EM data. The switching between EM and SEM should be carried out before the value of Φ reaches 2π. However, it is best to carry out the switching as soon as Φ or Φ^S is greater than π. This provides the largest buffer to the singularity and also ensures that the Φ never becomes much larger than π.

2.2 Hodographs

A hodograph is also known as a velocity diagram. Hodographs are not often used in contemporary research in Astrodynamics, but there are some excellent technical reports

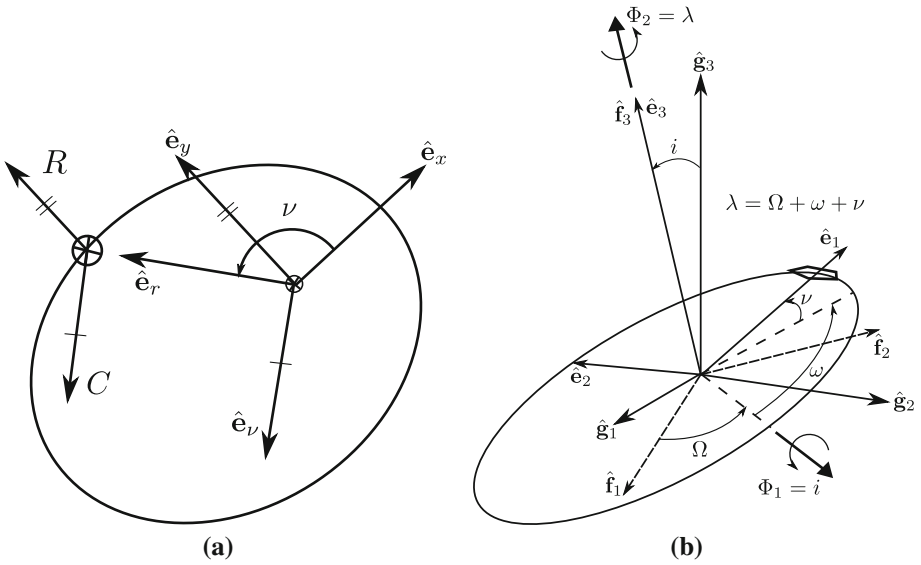

Fig. 2 Cartesian and polar frame on the orbital plane

on hodographs from the 1960s (Sun 1965; Altman 1965, 1967a,b; Eades 1968). More recent applications of hodographs include spacecraft rendezvous (Thompson et al. 2010), and problems in dynamics (Apostolatos 2003).

There are various methods to derive the hodographs, but we prefer the method found in Eades (1968) for its simplicity and elegance. The result is that the velocity at any point in an unperturbed orbit is the sum of a velocity normal to the radial vector laying in the orbital plane, C, and a velocity R, 90° ahead of the eccentricity vector. The eccentricity vector is the vector pointing from the focus of the orbit to the perifocus and is parallel to the unit vector $\hat{\mathbf{e}}_x$. This has been illustrated in Fig. 2a, which also gives the definition of a set of Cartesian and polar reference frames. In the Cartesian frame, $\hat{\mathbf{e}}_x$ points towards the perifocus of the orbit and $\hat{\mathbf{e}}_r$ points towards the orbiting body. C acts along $\hat{\mathbf{e}}_\nu$, which lies 90° ahead of $\hat{\mathbf{e}}_r$ in the orbital plane, and R acts along $\hat{\mathbf{e}}_y$.

According to Eades (1968), the two velocities have the magnitudes

$$C = \mu/h \tag{9}$$

$$R = \mu e/h = Ce \tag{10}$$

The hodographic velocities are very important for the USM as they are part of the state vector. We can also define a vector $\mathbf{R}$ that shows the direction in which R acts along and has the magnitude R.

$$\mathbf{R} = R\hat{\mathbf{e}}_y \tag{11}$$

Expressions for the velocities in the polar and Cartesian frame give rise to circles in both the Cartesian-velocity and the polar-velocity space. The path in the Cartesian-velocity space is known as the classical hodograph and the path in the polar-velocity space is known as the polar hodograph. According to Eades (1968), the equation for the classical hodograph is

$$v_x^2 + (v_y - R)^2 = C^2 \tag{12}$$

where v_x and v_y are the velocity components in the Cartesian reference frame. The classical hodograph is a circle with its center at $(v_x, v_y) = (0, R)$ and radius C. If orbits with constant C are chosen, which relates to constant angular momentum, the hodographs will have the same size, but their centers will translate up along the v_y-axis as the eccentricity increases.

The equation for the polar hodograph is

$$v_r^2 + (v_v - C)^2 = R^2 \tag{13}$$

The polar hodograph is a circle with its center at $(v_r, v_v) = (0, C)$ and radius R. If orbits with constant C are chosen, the hodographs will be concentric circles with the radius increasing with increasing eccentricity. The limiting case of circular orbits with $e = 0$ has a point as the polar hodograph.

3 The Unified State Model

Rotations and hodographs have been cursorily treated, because a basic knowledge of them is necessary in understanding the USM. The derivation starts using the notation of Keplerian elements for closed orbits, $e < 1$, but this is only for the sake of clarity. The only assumption made is that an osculating unperturbed Keplerian orbit exists at each moment in the orbit, and it does not matter if the orbit has $e \geq 1$, for the USM to hold. Thus, the equations of the USM are valid for any kind of conic section. Keplerian elements are first used to find the quaternions corresponding to $\mathcal{F}_f$ and $\mathcal{F}_e$; they are used because they give a deeper insight into the reference frames as they are relatively easy to visualize. These reference frames are:

$\mathcal{F}_g$, planetocentric inertial reference frame
$\mathcal{F}_f$, intermediate rotating reference frame
$\mathcal{F}_e$, rotating reference frame fixed to the orbiting body

The quaternion that describes the orientation of $\mathcal{F}_e$ with respect to $\mathcal{F}_g$ is only part of the state vector. The remaining part consists of the hodographic velocities, which were shown in Sect. 2.2. To fully utilize the USM, the dynamics of the velocity parameters and the kinematics of the quaternion have to be known. Thus, the time derivative of the various state elements is derived. It should be noted that the USM still describes the motion of the orbiting body in the inertial frame $\mathcal{F}_g$. The other rotating reference frames are simply used as mathematical tools to more easily express the vectors involved in the analysis.

3.1 Required reference frames

The USM quaternion is used to describe the orientation of $\mathcal{F}_e$ with respect to $\mathcal{F}_g$, see Fig. 2b. One intermediate frame, $\mathcal{F}_f$, is also used during the derivation and for expressing some elements of the final USM state vector. $\mathcal{F}_f$ is the resultant frame if $\mathcal{F}_g$ is rotated around the line of nodes, pointing towards the ascending node Ω, by an angle equal to the inclination i.

This means that the rotation can be expressed by the following Euler axis-angle pair:

$$\mathbf{a}_1 = \left[\cos\Omega,\ \sin\Omega,\ 0\right]^T \tag{14}$$

$$\Phi_1 = i \tag{15}$$

The corresponding quaternion can easily be constructed using the standard formulae, Eq. (1).

$$\boldsymbol{\epsilon}_1 = \left[\cos\Omega \sin(i/2),\ \sin\Omega \sin(i/2),\ 0\right]^T \tag{16}$$

$$\eta_1 = \cos(i/2) \tag{17}$$

It should be noted that for equatorial and circular orbits, Ω and ω are not defined, respectively. The USM still works for this case when the undefined Keplerian elements are set to 0. To get from $\mathcal{F}_f$ to $\mathcal{F}_e$, a rotation has to be carried out using the true longitude λ. λ is the sum of the right ascension of ascending node and the argument of latitude, u.

$$\lambda = \Omega + u = \Omega + \omega + \nu \tag{18}$$

In $\mathcal{F}_f$, this rotation can be expressed by the Euler axis-angle pair

$$\mathbf{a}_2 = \left[0,\ 0,\ 1\right]^T \tag{19}$$

$$\Phi_2 = \lambda \tag{20}$$

Using the Euler axis-angle pair, the quaternion that expresses the rotation from $\mathcal{F}_f$ to $\mathcal{F}_e$ can again be easily extracted:

$$\boldsymbol{\epsilon}_2 = \left[0,\ 0,\ \sin(\lambda/2)\right]^T \tag{21}$$

$$\eta_2 = \cos(\lambda/2) \tag{22}$$

The desired quaternion $(\boldsymbol{\epsilon}_3, \eta_3)$ is the one that describes the rotation between $\mathcal{F}_g$ and $\mathcal{F}_e$. This is the result of two successive rotations, first $(\boldsymbol{\epsilon}_1, \eta_1)$ followed by $(\boldsymbol{\epsilon}_2, \eta_2)$ (Hughes 1986).

$$\boldsymbol{\epsilon}_3 = \begin{bmatrix} \sin(i/2)\,(\cos\Omega\cos(\lambda/2) + \sin\Omega\sin(\lambda/2)) \\ \sin(i/2)\,(\sin\Omega\cos(\lambda/2) - \cos\Omega\sin(\lambda/2)) \\ \cos(i/2)\sin(\lambda/2) \end{bmatrix} \tag{23}$$

$$\eta_3 = \cos(i/2)\cos(\lambda/2) \tag{24}$$

It should be noted that the elements of the quaternion are not in the same form as found in Altman (1972), Chodas (1981). To get to the desired form, λ should be substituted by the sum of its two constituents: Ω and u. Finally, some simplification has to be done using the sum of angles trigonometric formulae to reach the desired form of the quaternion. Since quaternion $(\boldsymbol{\epsilon}_3, \eta_3)$ describes the orientation of the orbital frame $\mathcal{F}_e$ with respect to $\mathcal{F}_g$, it is renamed to $(\boldsymbol{\epsilon}_O, \eta_O)$.

$$\begin{bmatrix} \boldsymbol{\epsilon}_O \\ \eta_O \end{bmatrix} = \begin{bmatrix} \sin\frac{i}{2}\cos\left(\frac{\Omega-u}{2}\right) \\ \sin\frac{i}{2}\sin\left(\frac{\Omega-u}{2}\right) \\ \cos\frac{i}{2}\sin\left(\frac{\Omega+u}{2}\right) \\ \cos\frac{i}{2}\cos\left(\frac{\Omega+u}{2}\right) \end{bmatrix} \tag{25}$$

3.2 Velocities

The quaternion accounts for four out of the seven elements of the USM state vector. However, only the information about the orientation of the orbital plane and the angular location of the orbiting body can be found from the quaternion. To get information on the size and shape of the orbit, the hodograph parameters have to be used.

The hodograph quantities that the USM uses are C, R_{f1}, and R_{f2}. R_{f1} and R_{f2} are simply the components of $\mathbf{R}$ expressed in $\mathcal{F}_f$. Since there is no out-of-plane velocity component in an orbit, R_{f3} is 0. Knowing that C acts in the direction of $\hat{\mathbf{e}}_2$, and R acts in the direction of $\hat{\mathbf{e}}_1$ when $\nu = 90°$, the velocities expressed in $\mathcal{F}_e$ at any point in the orbit are

$$v_{e1} = R_{f1}\cos\lambda + R_{f2}\sin\lambda \tag{26}$$

$$v_{e2} = C - R_{f1}\sin\lambda + R_{f2}\cos\lambda \tag{27}$$

$$v_{e3} = 0 \tag{28}$$

It is important to know the velocities expressed in $\mathcal{F}_e$, as they are used further in the derivation. Also, some perturbing forces like atmospheric drag depend on the velocity. Given v_{e1}, v_{e2}, λ, and C, R_{f1} and R_{f2} can be computed by the inverse transformation of Eqs. (26) and (27).

$$\begin{bmatrix} R_{f1} \\ R_{f2} \end{bmatrix} = \begin{bmatrix} \cos\lambda \\ \sin\lambda \end{bmatrix} v_{e1} + \begin{bmatrix} -\sin\lambda \\ \cos\lambda \end{bmatrix} v_{e2} + \begin{bmatrix} \sin\lambda \\ -\cos\lambda \end{bmatrix} C \tag{29}$$

It can be seen that the sine and cosine of λ are very important parameters for the velocity and can be computed from the Keplerian elements. However, a relation for them in terms of the USM elements still has to be found. In the quaternion elements ϵ_{O3} and η_O from Eq. (23) and Eq. (24), respectively, the half-angle sine and cosines of λ are present. After rearranging, the following relations about the half-angle of λ can be derived:

$$\sin(\lambda/2) = \frac{\epsilon_{O3}}{\cos(i/2)} \tag{30a}$$

$$\cos(\lambda/2) = \frac{\eta_O}{\cos(i/2)} \tag{30b}$$

$$\tan(\lambda/2) = (\epsilon_{O3}/\eta_O) \tag{30c}$$

Trigonometric half-angle formulae have to be used to get relations of $\cos\lambda$ using $\cos^2(\lambda/2)$ and $\sin^2(\lambda/2)$. Combining with Eq. (30c) gives

$$(\epsilon_{O3}/\eta_O)^2 = (1-\cos\lambda)/(1+\cos\lambda) \tag{31}$$

Equation (31) can then be solved for $\cos\lambda$.

$$\cos\lambda = (\eta_O^2 - \epsilon_{O3}^2)/(\epsilon_{O3}^2 + \eta_O^2) \tag{32}$$

The tangent of λ can be found from Eq. (30c) to be:

$$\tan\lambda = 2\,(\epsilon_{O3}\eta_O)\,/\,\left(\eta_O^2 - \epsilon_{O3}^2\right) \tag{33}$$

With the tangent and the cosine of λ known, the sine is found to be

$$\sin\lambda = (2\epsilon_{O3}\eta_O)/(\epsilon_{O3}^2 + \eta_O^2) \tag{34}$$

3.3 Kinematics and dynamics

So far, all the USM state elements have been presented and explained. To be able to utilize the USM, the time derivatives of the quaternion and the velocities have to be derived. For this purpose, it is useful to first find the vector from the center of the attracting body to the orbiting body. This is the radius vector $\mathbf{r}$, and according to the definition of $\mathcal{F}_e$, it lies in the direction of $\hat{\mathbf{e}}_1$.

$$\mathbf{r} = r\hat{\mathbf{e}}_1 \tag{35}$$

In Eq. (35), r is the magnitude of the radius vector. This parameter can also be derived from the given information. The angular momentum, $\mathbf{h}$, lies along $\hat{\mathbf{e}}_3$, and the orbiting body has no velocity component along $\hat{\mathbf{e}}_3$. This results in the following equation for the angular momentum:

$$h\hat{\mathbf{e}}_3 = r v_{e2}\hat{\mathbf{e}}_3 \tag{36}$$

Rearranging Eq. (36) and using Eq. (9) gives an expression for $\mathbf{r}$ expressed in $\mathcal{F}_e$.

$$\mathbf{r} = \mu/(C v_{e2})\hat{\mathbf{e}}_1 \tag{37}$$

The acceleration that the body experiences can be split up into the central gravitational attraction, $\mathbf{a}_g$, and the perturbing acceleration, $\mathbf{a}_e$. This perturbing acceleration is expressed in $\mathcal{F}_e$. The acceleration due to uniform gravity is

$$\mathbf{a}_g = -\mu/r^3\mathbf{r} = -\mu/r^2\hat{\mathbf{e}}_1 = -C^2 v_{e2}^2/\mu\hat{\mathbf{e}}_1 \tag{38}$$

and $\mathbf{a}_e$ is defined as

$$\mathbf{a}_e = a_{e1}\hat{\mathbf{e}}_1 + a_{e2}\hat{\mathbf{e}}_2 + a_{e3}\hat{\mathbf{e}}_3 \tag{39}$$

The total acceleration is

$$\mathbf{a} = \left(a_{e1} - C^2 v_{e2}^2/\mu\right)\hat{\mathbf{e}}_1 + a_{e2}\hat{\mathbf{e}}_2 + a_{e3}\hat{\mathbf{e}}_3 \tag{40}$$

The quaternion time derivative is a standard formula based on the quaternion and the angular velocities (Schaub and Junkins 2002).

$$\begin{bmatrix} \dot{\boldsymbol{\epsilon}} \\ \dot{\eta} \end{bmatrix} = \frac{1}{2}\begin{bmatrix} 0 & \omega_3 & -\omega_2 & \omega_1 \\ -\omega_3 & 0 & \omega_1 & \omega_2 \\ \omega_2 & -\omega_1 & 0 & \omega_3 \\ -\omega_1 & -\omega_2 & -\omega_3 & 0 \end{bmatrix}\begin{bmatrix} \boldsymbol{\epsilon} \\ \eta \end{bmatrix} \tag{41}$$

These angular velocity components will be solved for as we go through the derivation.

We begin the derivation by taking the time derivative of the velocity in $\mathcal{F}_e$. It should be noted that $\mathcal{F}_e$ is a rotating frame of reference and therefore, the velocity derivative is

$$\dot{\mathbf{v}} = \left.\frac{\mathrm{d}\mathbf{v}}{\mathrm{d}t}\right|_{\mathcal{F}_e} + \boldsymbol{\omega} \times \mathbf{v} \tag{42}$$

so

$$\begin{aligned} \dot{\mathbf{v}} = &\left(\dot{v}_{e1} - v_{e2}\omega_3\right)\hat{\mathbf{e}}_1 + \left(\dot{v}_{e2} + v_{e1}\omega_3\right)\hat{\mathbf{e}}_2 \\ &+ \left(v_{e2}\omega_1 - v_{e1}\omega_2\right)\hat{\mathbf{e}}_3 \end{aligned} \tag{43}$$

To get to Eq. (43), use was made of the fact that $v_{e3} = \dot{v}_{e3} = 0$. Knowing that the time derivative of the velocity in Eq. (43) has to equal the total acceleration in Eq. (40), the scalar velocity time derivative components can be found to be

$$\dot{v}_{e1} = a_{e1} - \left(C^2 v_{e2}^2/\mu\right) + v_{e2}\omega_3 \tag{44}$$

$$\dot{v}_{e2} = a_{e2} - v_{e1}\omega_3 \tag{45}$$

Also,

$$a_{e3} = v_{e2}\omega_1 - v_{e1}\omega_2 \tag{46}$$

Similarly, the position vector from Eq. (37) can also be differentiated with respect to time.

$$\begin{aligned}\dot{\mathbf{r}} = &-\mu\left(\dot{C}/\left(C^2 v_{e2}\right) + \dot{v}_{e2}/\left(C v_{e2}^2\right)\right)\hat{\mathbf{e}}_1 \\ &+\mu\Big(\omega_3/\left(C v_{e2}\right)\Big)\hat{\mathbf{e}}_2 - \mu\Big(\omega_2/\left(C v_{e2}\right)\Big)\hat{\mathbf{e}}_3\end{aligned} \tag{47}$$

Since the time derivative of the position is the velocity, consisting of only v_{e1} and v_{e2}, the values of certain unknown parameters can be found.

$$\omega_2 = 0 \tag{48}$$

$$\omega_3 = C v_{e2}^2/\mu \tag{49}$$

$$\dot{C} = -C a_{e2}/(v_{e2}) \tag{50}$$

By using Eqs. (48) and (46), the remaining angular velocity, ω_1, can be found.

$$\omega_1 = a_{e3}/v_{e2} \tag{51}$$

A new parameter p is now defined as:

$$p = C/v_{e2} \tag{52}$$

This results in $\dot{C}$ being

$$\dot{C} = -p a_{e2} \tag{53}$$

The dynamics of the two remaining USM elements still have to be derived, i.e., $\dot{R}_{f1}$ and $\dot{R}_{f2}$. First, the time derivative of Eq. (29) has to be taken.

$$\dot{R}_{f1} = \dot{v}_{e1}\cos\lambda + \left(\dot{C} - \dot{v}_{e2}\right)\sin\lambda - \dot{\lambda} R_{f2} \tag{54}$$

$$\dot{R}_{f2} = \dot{v}_{e1}\sin\lambda + \left(\dot{v}_{e2} - \dot{C}\right)\cos\lambda + \dot{\lambda} R_{f1} \tag{55}$$

In Eqs. (54) and (55), all parameters except for $\dot{\lambda}$ are known. The cosine and sine of λ are known from Eqs. (32) and (34), respectively, which are based on the quaternion elements. The time derivative of the quaternion is known from the standard equation and so, the time derivatives of the cosine and sine of λ can be computed. It is only necessary to compute the time derivative in terms of USM elements of one of the trigonometric functions. For example, if the time derivative of $\sin\lambda$ is computed, $\dot{\lambda}$ can be computed using the reversed chain rule in the following way

$$\dot{\lambda} = \frac{1}{\cos\lambda}\frac{\mathrm{d}}{\mathrm{d}t}\left(\sin\lambda\right) \tag{56}$$

In Eq. (56), the time derivative of $\sin\lambda$ can be computed, using the fact that $\sin\lambda$ depends on ϵ_{O3} and η, in the following manner:

$$\frac{\mathrm{d}}{\mathrm{d}t}\left(\sin\lambda\right) = \frac{\partial\sin\lambda}{\partial\epsilon_{O3}}\dot{\epsilon}_{O3} + \frac{\partial\sin\lambda}{\partial\eta_O}\dot{\eta}_O \tag{57}$$

The partials of $\sin\lambda$ with respect to ϵ_{O3} and η_O are, using Eq. (34)

$$\frac{\partial\sin\lambda}{\partial\epsilon_{O3}} = 2\eta_O\left(\eta_O^2 - \epsilon_{O3}^2\right)/\left(\epsilon_{O3}^2 + \eta_O^2\right)^2 \tag{58a}$$

$$\frac{\partial\sin\lambda}{\partial\eta_O} = -2\epsilon_{O3}\left(\eta_O^2 - \epsilon_{O3}^2\right)/\left(\epsilon_{O3}^2 + \eta_O^2\right)^2 \tag{58b}$$

Filling in the partials from Eq. (58), the time derivatives of the individual quaternion elements, and $\cos\lambda$ from Eq. (32) into Eq. (56) followed by some algebraic manipulation leads to

$$\dot{\lambda} = \frac{\epsilon_{O1}\epsilon_{O3} - \epsilon_{O2}\eta_O}{\epsilon_{O3}^2 + \eta_O^2}\omega_1 + \omega_3 \tag{59}$$

For ease of notation, a new parameter γ is introduced as the coefficient to ω_1:

$$\gamma = \frac{\epsilon_{O1}\epsilon_{O3} - \epsilon_{O2}\eta_O}{\epsilon_{O3}^2 + \eta_O^2} \tag{60}$$

Finally, after substitution of Eqs. (59–60) into Eqs. (54–55), the time derivatives of R_{f1} and R_{f2} can be written as

$$\dot{R}_{f1} = a_{e1}\cos\lambda - a_{e2}(1+p)\sin\lambda - a_{e3}\left(\gamma R_{f2}/v_{e2}\right) \tag{61}$$

$$\dot{R}_{f2} = a_{e1}\sin\lambda + a_{e2}(1+p)\cos\lambda + a_{e3}\left(\gamma R_{f1}/v_{e2}\right) \tag{62}$$

The original model found in Altman (1972), wrongly assumes that $\dot{\lambda} = \omega_3$. This erroneous assumption removes the dependency of the hodograph parameters on the out-of-plane perturbations. This error was pointed out in Chodas (1981) and the correct equations were also shown in Raol and Sinha (1985), but neither of these papers show any derivation of the correction. The dependance of $\dot{\lambda}$ on a_{e3} follows from the fact that $\dot{\lambda}$ depends on $\dot{\epsilon}_{O3}$ and $\dot{\eta}_O$, which both depend on ω_1, which ultimately depends on a_{e3}.

Summarized, the dynamics of the hodograph parameters of the USM can be expressed in a canonical form as

$$\begin{bmatrix} \dot{C} \\ \dot{R}_{f1} \\ \dot{R}_{f2} \end{bmatrix} = \begin{bmatrix} 0 & -p & 0 \\ \cos\lambda & -(1+p)\sin\lambda & -\gamma R_{f2}/v_{e2} \\ \sin\lambda & (1+p)\cos\lambda & \gamma R_{f1}/v_{e2} \end{bmatrix} \begin{bmatrix} a_{e1} \\ a_{e2} \\ a_{e3} \end{bmatrix} \tag{63}$$

Finally, we can define the complete USM state in the following way

$$\mathbf{x} = \begin{bmatrix} C & R_{f1} & R_{f2} & \epsilon_{O1} & \epsilon_{O2} & \epsilon_{O3} & \eta_O \end{bmatrix}^T \tag{64}$$

The time derivative of this state is a function of the present state and any perturbing accelerations, $\dot{\mathbf{x}} = f(\mathbf{x}, \mathbf{a}_e)$. To compute the time derivative, the following quantities have to be computed first: ω_1, ω_3, v_{e2}, and γ, see Eqs. (51), (49), (27), and (60), respectively. The parameter p should be computed thereafter since it requires the value of v_{e2}, Eq. (52). Using all these parameters, the time derivatives of the quaternion elements and of the hodograph velocities can be calculated. See Eqs. (41) and (63).

3.4 Implementing the USM

In the previous sections, the elegant USM has been completely derived. The error in the original model, pointed out in Chodas (1981), has been validated. Many important conclusions about the USM have been made in Altman (1972), and Chodas (1981). These will not be repeated here, except for the singularities in the USM. There are two cases where this singularity occurs. The first case is when the angular momentum is 0. In this case, the orbit is a degenerate conic section and C is singular. This would not happen in the usual case for orbits, except for hyperbolic orbits when the true-anomaly limit is effectively reached. At this point, the motion becomes linear. If the patched conic approximation is used along with the sphere of influence of the Earth, it is found that the true anomaly is under the true

anomaly limit for most hyperbolic orbits. The true anomaly is, however, very close to the true-anomaly limit, which would mean that ω_3 is very small. Thus, the integration may not be very accurate.

The second singularity occurs if the orbit is retrograde with $i = 180°$. In this case $\eta_O = 0$ and $\epsilon_{O3} = 0$. When the orbit is equatorial, Ω is not defined and so it should not have an effect on the state elements. For an equatorial prograde orbit, $\mathbf{C}_{f,g} = \mathbf{I}_3$ and Ω indeed does not have any effect. For a retrograde orbit, the value of $\mathbf{C}_{f,g}$ depends on Ω. Thus, for different values of Ω, there will be a different DCM, effectively representing the same orbit. There is a method to circumvent this problem, shown in Chodas (1981), by rotating around the line of descending nodes. This method will, however, not be dealt with in this paper.

A typical user would have the initial conditions of an orbit to be integrated in Cartesian coordinates or Keplerian elements. The conversion from the Keplerian elements to the USM state can be carried out by using the equations found in Sects. 3.1 and 3.2. The conversion from a initial condition set in Cartesian coordinates to the USM, can also be carried out in a fairly straight forward manner. This conversion is similar to the one found in Chodas (1981), but with a different method for extracting the quaternion.

The state in Cartesian coordinates consists of the position given in (x, y, z), and the velocity (v_x, v_y, v_z). This position and velocity are written as vectors $\mathbf{r}$ and $\mathbf{v}$, respectively. The first step is to calculate the angular momentum, which is required for computing C.

$$\mathbf{h} = \begin{bmatrix} h_x \\ h_y \\ h_z \end{bmatrix} = \begin{bmatrix} x \\ y \\ z \end{bmatrix} \times \begin{bmatrix} v_x \\ v_y \\ v_z \end{bmatrix} = \begin{bmatrix} yv_z - zv_y \\ zv_x - xv_z \\ xv_y - yv_x \end{bmatrix} \tag{65}$$

C can be found from

$$C = \frac{\mu}{h} \tag{66}$$

where h is the magnitude of the angular momentum found in Eq. (65).

The velocity can be split up into $\mathbf{v}_{e1}$ and $\mathbf{v}_{e2}$ in the following way

$$\mathbf{v}_{e1} = \frac{\mathbf{r}^T\mathbf{v}}{r^2}\mathbf{r} = \frac{xv_x + yv_y + zv_z}{x^2 + y^2 + z^2} \begin{bmatrix} x \\ y \\ z \end{bmatrix} \tag{67a}$$

$$\mathbf{v}_{e2} = \mathbf{v} - \mathbf{v}_{e1} \tag{67b}$$

In Eq. (67), $\mathbf{v}_{e1}$ is simply the projection of $\mathbf{v}$ along the radial vector $\mathbf{r}$. In Eq. (67), $\mathbf{v}_{e1}$ and $\mathbf{v}_{e2}$ are still expressed $\mathcal{F}_g$. They are simply computed in vectorial form to be able to extract the scalar magnitudes v_{e1} and v_{e2}.

The quaternion can be extracted from a DCM from $\mathcal{F}_g$ to $\mathcal{F}_e$ created using the state expressed in Cartesian coordinates. The three unit vectors that make $\mathcal{F}_g$ are

$$\hat{\mathbf{g}}_1 = \begin{bmatrix} 1 \\ 0 \\ 0 \end{bmatrix} \quad \hat{\mathbf{g}}_2 = \begin{bmatrix} 0 \\ 1 \\ 0 \end{bmatrix} \quad \hat{\mathbf{g}}_3 = \begin{bmatrix} 0 \\ 0 \\ 1 \end{bmatrix} \tag{68}$$

The three unit vectors that make $\mathcal{F}_e$, expressed in $\mathcal{F}_g$ are then

$$\hat{\mathbf{e}}_1 = \frac{\mathbf{r}}{|\mathbf{r}|} \quad \hat{\mathbf{e}}_3 = \frac{\mathbf{h}}{|\mathbf{h}|} \quad \hat{\mathbf{e}}_2 = \hat{\mathbf{e}}_3 \times \hat{\mathbf{e}}_1 = \frac{\mathbf{h} \times \mathbf{r}}{|\mathbf{h} \times \mathbf{r}|} \tag{69}$$

which can then be expanded to give

$$\hat{\mathbf{e}}_1 = \frac{1}{r}\begin{bmatrix} x \\ y \\ z \end{bmatrix} \qquad \hat{\mathbf{e}}_2 = -\frac{1}{rh}\begin{bmatrix} zh_y - yh_z \\ xh_z - zh_x \\ yh_x - xh_y \end{bmatrix} \qquad \hat{\mathbf{e}}_3 = \frac{1}{h}\begin{bmatrix} h_x \\ h_y \\ h_z \end{bmatrix} \tag{70}$$

From the definition of a DCM (Hughes 1986), the elements of $\mathbf{C}_{e,g}$, $c_{i,j}$, can be found in the following manner

$$\hat{\mathbf{e}}_1 = c_{1,1}\hat{\mathbf{g}}_1 + c_{1,2}\hat{\mathbf{g}}_2 + c_{1,3}\hat{\mathbf{g}}_3 \tag{71a}$$

$$\hat{\mathbf{e}}_2 = c_{2,1}\hat{\mathbf{g}}_1 + c_{2,2}\hat{\mathbf{g}}_2 + c_{2,3}\hat{\mathbf{g}}_3 \tag{71b}$$

$$\hat{\mathbf{e}}_3 = c_{3,1}\hat{\mathbf{g}}_1 + c_{3,2}\hat{\mathbf{g}}_2 + c_{3,3}\hat{\mathbf{g}}_3 \tag{71c}$$

Solving for all the elements of the rotation matrix results in

$$\mathbf{C}_{e,g} = \frac{1}{rh}\begin{bmatrix} xh & yh & zh \\ zh_y - yh_z & xh_z - zh_x & yh_x - xh_y \\ rh_x & rh_y & rh_z \end{bmatrix} \tag{72}$$

The quaternion can then be extracted from the DCM using any standard singularity-free technique (Hughes 1986; Schaub and Junkins 2002).

Finally, the velocities R_{f1} and R_{f2} can be found using

$$R_{f1} = v_{e1}\cos\lambda - (v_{e2} - C)\sin\lambda \tag{73a}$$

$$R_{f2} = v_{e1}\sin\lambda + (v_{e2} - C)\cos\lambda \tag{73b}$$

In the above equations, $\cos\lambda$ and $\sin\lambda$ can be found from quaternion elements given in Eqs. (32) and (34), respectively.

3.5 Summary of the equations used in the USM

After an instance of a state of the USM has been initialized using the above equations, the state derivative requires the following computations that are spread throughout the derivation and are repeated here for the sake of clarity.

$$\begin{bmatrix} \sin\lambda \\ \cos\lambda \end{bmatrix} = \frac{1}{\epsilon_{O3}^2 + \eta_O^2}\begin{bmatrix} 2\epsilon_{O3}\eta_O \\ \eta_O^2 - \epsilon_{O3}^2 \end{bmatrix} \tag{74}$$

$$\lambda = \text{atan2}\left(\sin\lambda, \cos\lambda\right) \tag{75}$$

$$\begin{bmatrix} v_{e1} \\ v_{e2} \end{bmatrix} = \begin{bmatrix} 0 \\ C \end{bmatrix} + \begin{bmatrix} \cos\lambda & \sin\lambda \\ -\sin\lambda & \cos\lambda \end{bmatrix}\begin{bmatrix} R_{f1} \\ R_{f2} \end{bmatrix} \tag{76}$$

$$p = \frac{C}{v_{e2}} \tag{77}$$

$$\gamma = \frac{\epsilon_{O1}\epsilon_{O3} - \epsilon_{O2}\eta_O}{\epsilon_{O3}^2 + \eta_O^2} \tag{78}$$

$$\omega_1 = \frac{a_{e3}}{v_{e2}} \tag{79}$$

$$\omega_3 = \frac{Cv_{e2}^2}{\mu} \tag{80}$$

$$\begin{bmatrix} \dot{C} \\ \dot{R}_{f1} \\ \dot{R}_{f2} \end{bmatrix} = \begin{bmatrix} 0 & -p & 0 \\ \cos\lambda & -(1+p)\sin\lambda & -\gamma R_{f2}/v_{e2} \\ \sin\lambda & (1+p)\cos\lambda & \gamma R_{f1}/v_{e2} \end{bmatrix}\begin{bmatrix} a_{e1} \\ a_{e2} \\ a_{e3} \end{bmatrix} \tag{81}$$

$$\begin{bmatrix} \dot{\epsilon}_{O1} \\ \dot{\epsilon}_{O2} \\ \dot{\epsilon}_{O3} \\ \dot{\eta}_O \end{bmatrix} = \frac{1}{2} \begin{bmatrix} 0 & \omega_3 & 0 & \omega_1 \\ -\omega_3 & 0 & \omega_1 & 0 \\ 0 & -\omega_1 & 0 & \omega_3 \\ -\omega_1 & 0 & -\omega_3 & 0 \end{bmatrix} \begin{bmatrix} \epsilon_{O1} \\ \epsilon_{O2} \\ \epsilon_{O3} \\ \eta_O \end{bmatrix} \tag{82}$$

4 Modifications to the Unified State Model

If a USM state is considered as using three velocity hodograph parameters and information expressing the orientation of the orbital frame with respect to the central body frame, it is possible to make modifications while remaining under the framework of the USM. The original USM proposed by Altman uses quaternions to represent the orientation of the orbital frame. However, other parameter sets such as Euler angles, the Euler axis-angle, Rodrigues parameters, and Cayley-Klein parameters could also be used. In this work, we suggest two modified versions of the USM using the modified Rodrigues parameters and the Euler axis-angle method (also known as exponential mapping) to express the orientation of the orbital frame.

4.1 Unified State Model using modified Rodrigues parameters

The USM has seven elements, of which four are the elements of a quaternion. Since the quaternion is used to describe the orientation of the orbital frame, any other set of attitude parameters should also suffice. According to Schaub and Junkins (2002), any attitude parameter set that has fewer than four elements will have a singularity. MRP, however, have the benefit of having shadow parameters that allow bypassing this singularity. This is also true for Euler angles, but they have the disadvantage of having trigonometric functions that are computationally costly. Thus, we propose a method of using MRP to reduce the number of elements of the USM theory to six. As mentioned before, the classical USM will be referred to as USM7 and the USM using MRP will be referred to as USM6.

Since MRP are used to describe the rotation instead of a quaternion, all the equations of the USM7 that contain quaternion elements have to converted to the MRP. The conversion from quaternion to MRP and SMRP and vice versa is done using Eqs. (83) and (84), respectively.

$$\boldsymbol{\sigma} = \frac{\boldsymbol{\epsilon}}{1+\eta}, \forall \eta \neq -1 \tag{83}$$

$$\boldsymbol{\sigma}^S = \frac{-\boldsymbol{\epsilon}}{1-\eta}, \forall \eta \neq 1 \tag{84}$$

It is now possible to convert the quaternion of the orbital frame to an MRP and SMRP vector. This is carried out by plugging the expression for the quaternion from Eq. (25) into Eqs. (83) and (84), yielding:

$$\boldsymbol{\sigma}_O = \left(1 + \cos\left(\frac{i}{2}\right)\cos\left(\frac{\Omega+u}{2}\right)\right)^{-1} \begin{bmatrix} \sin\left(\frac{i}{2}\right)\cos\left(\frac{\Omega-u}{2}\right) \\ \sin\left(\frac{i}{2}\right)\sin\left(\frac{\Omega-u}{2}\right) \\ \cos\left(\frac{i}{2}\right)\sin\left(\frac{\Omega+u}{2}\right) \end{bmatrix} \tag{85}$$

$$\boldsymbol{\sigma}_O^S = \left(\cos\left(\frac{i}{2}\right)\cos\left(\frac{\Omega+u}{2}\right) - 1\right)^{-1} \begin{bmatrix} \sin\left(\frac{i}{2}\right)\cos\left(\frac{\Omega-u}{2}\right) \\ \sin\left(\frac{i}{2}\right)\sin\left(\frac{\Omega-u}{2}\right) \\ \cos\left(\frac{i}{2}\right)\sin\left(\frac{\Omega+u}{2}\right) \end{bmatrix} \tag{86}$$

The rest of the equations will be the same, because they represent the dynamics in the orbital frame, which has the same orientation expressed in quaternions and MRP. The only differences will be the components that are computed from the quaternions. These are: λ, γ, and the kinematic differential equation, Eq. (41).

The required relations for the sine and cosine of λ are:

$$\begin{bmatrix} \sin\lambda \\ \cos\lambda \end{bmatrix} = \frac{1}{4\sigma_3^2 + \left(1-\sigma^2\right)^2} \begin{bmatrix} 4\sigma_3\left(1-\sigma^2\right) \\ \left(1-\sigma^2\right)^2 - 4\sigma_3^2 \end{bmatrix} \tag{87}$$

The kinematic differential equation in terms of MRP and SMRP using the fact that $\omega_2 = 0$ becomes:

$$\dot{\boldsymbol{\sigma}} = \frac{1}{4} \begin{bmatrix} \left(1-\sigma^2+2\sigma_1^2\right)\omega_1 + 2(\sigma_1\sigma_3+\sigma_2)\omega_3 \\ 2(\sigma_2\sigma_1+\sigma_3)\omega_1 + 2(\sigma_2\sigma_3-\sigma_1)\omega_3 \\ 2(\sigma_3\sigma_1-\sigma_2)\omega_1 + \left(1-\sigma^2+2\sigma_3^2\right)\omega_3 \end{bmatrix} \tag{88}$$

The procedure of computing $\dot{\lambda}$ is the same as for USM7 and can be carried out in the following way:

$$\dot{\lambda} = \frac{1}{\cos\lambda}\left(\frac{\partial \sin\lambda}{\partial\sigma_1}\dot{\sigma_1} + \frac{\partial \sin\lambda}{\partial\sigma_2}\dot{\sigma_2} + \frac{\partial \sin\lambda}{\partial\sigma_3}\dot{\sigma_3}\right) \tag{89}$$

The relation for $\dot{\lambda}$ is then:

$$\dot{\lambda} = \frac{2\left(\sigma_2^3 + \sigma_1^2\sigma_2 + \sigma_2\sigma_3^2 + 2\sigma_1\sigma_3 - \sigma_2\right)}{\sigma_1^4 + \sigma_2^4 + \sigma_3^4 + 2\left(\sigma_1^2\sigma_2^2 + \sigma_1^2\sigma_3^2 + \sigma_2^2\sigma_3^2 - \sigma_1^2 - \sigma_2^2 + \sigma_3^2\right) + 1}\omega_1 + \omega_3 \tag{90}$$

The equations presented above for the MRP also hold for the SMRP because both the time-derivative equations and the equations for the sine and cosine of λ are the same.

When using the USM6, it is important to keep track of wether MRP or SMRP are being used. This can be done by adding an extra flag element to the state. After each integration step, the norm σ of the MRP or SMRP vector should be computed. In case $\sigma > 1$, the type of MRP has to be switched. The procedure outlined in this section for using MRP instead of quaternions, can also be used to express the USM in terms of any other attitude parameter.

4.2 Unified State Model using exponential mapping

This proposed modification of the USM is called the Unified State Model using exponential mapping (USMEM). The complete state vector for this method also consists of six elements like the USM6. The first three elements are again the hodographic velocities and the last three elements are the EM vector.

The conversion between EM and its "shaded" counterpart SEM to quaternion is the same and therefore, we propose to not keep track of the type of EM. It is only necessary to keep track if we need to interpolate using the EM parameters. Thus, the EM is initialized from the conversion of the quaternion, Eq. (5). For the dynamics, the EM is converted to a quaternion to find $\dot{C}$, $\dot{R}_{f1}$, $\dot{R}_{f2}$, and $\boldsymbol{\omega}$ in the same manner as for the USM7, Eq. (6). The time derivative of the EM vector, $\dot{\mathbf{a}}$, can then be computed.

The time derivative of the EM vector can be written in two forms. One form according to Schaub and Junkins (2002) is

$$\dot{\mathbf{a}} = \left(\mathbf{I}_3 + \frac{[\mathbf{a}\times]}{2} + \frac{1}{\Phi^2}\left(1 - \frac{\Phi}{2}\cot\frac{\Phi}{2}\right)[\mathbf{a}\times][\mathbf{a}\times]\right)\boldsymbol{\omega} \tag{91}$$

The other form found in Grassia (1998), which can be derived from Eq. (91) is

$$\dot{\mathbf{a}} = \frac{1}{2}\left(\Phi \cot\frac{\Phi}{2}\boldsymbol{\omega} - \boldsymbol{\omega}\times\mathbf{a} - \frac{\boldsymbol{\omega}\cdot\mathbf{a}}{\Phi}\left(\cot\frac{\Phi}{2} - \frac{2}{\Phi}\right)\mathbf{a}\right) \tag{92}$$

To get from Eq. (91) to (92), the vector triple cross product rule has to be used which gives

$$[\mathbf{a}\times][\mathbf{a}\times]\boldsymbol{\omega} = \mathbf{a}(\mathbf{a}\cdot\mathbf{a}) - \Phi^2\boldsymbol{\omega} \tag{93}$$

Both Eqs. (91) and (92) have a singularity at $\Phi = 0$. A method to bypass this singularity using the Taylor series expansion is given in Grassia (1998) to be

$$\dot{\mathbf{a}} \approx \frac{1}{2}\left(\frac{12-\Phi^2}{6}\boldsymbol{\omega} - \boldsymbol{\omega}\times\mathbf{a} - \boldsymbol{\omega}\cdot\mathbf{a}\left(\frac{60+\Phi^2}{360}\right)\mathbf{a}\right) \tag{94}$$

It should be noted that Eqs. (92) and (94) found in Grassia (1998) originally have a typo where there is a '+' preceding $\boldsymbol{\omega}\times\mathbf{a}$ instead of a '−'.

Testing Eqs. (91) and (92) in MATLAB shows that Eq. (91) has better numerical accuracy than Eq. (92). However, Eq. (94) should be used when Φ is close to 0.

5 Simulations and results

It is important to put all the theoretical equations to practice to investigate the numerical performance of the USM. The simulations are carried out using USM7, USM6, USMEM, and Cartesian coordinates. Simulations of unperturbed Keplerian orbits will not be shown as they are not realistic scenarios for real missions; they were only used for software verification. Some simulations of unperturbed orbits were carried out to check and validate the USM models and it was found that the error is many orders of magnitude lower for the USM than for the Cartesian coordinates. By integration in Cartesian coordinates, we imply Cowell's method and Runge-Kutta type integrators. Runge-Kutta type integrators are used even though Cowell's method is more suited for multi-step integrators such as Störmer-Cowell routines, because the multi-step integrators are harder to start and implement, especially the variable step-size variants. Therefore, most users simply use the Runge-Kutta type of integrators.

To be able to fully apply and analyze the USM, tests were carried out with perturbed orbits. Using low-thrust propulsion to change orbital parameters is the focus of many orbit studies nowadays. There are a few analytical solutions for low-thrust orbits such as exponential sinusoids or *exposins* (Petropoulos and Longuski 2004). These analytical solutions suffice for a first-order approximation, but to get more accurate results, optimizers have to be used that simulate the whole trajectory. However, low-thrust orbits take a long time to simulate because of the mission duration. Therefore, the USM could be readily applied if the CPU time for simulations decreases. Since there have been many interplanetary missions to Mars with many more to come, a Mars aerobraking scenario has also been implemented to investigate the applicability of the USM.

Apart from the relative tests, the USM will be compared using test cases available in Bond and Allman (1996), which gives some insight into the absolute performance. An extra comparison will be carried out where the only perturbation present is the inhomogeneity of the Earth's gravity field. The gravity forces vary rapidly along the orbit if higher-order (in our case 70×70) spherical harmonics are used. This could remove the advantage that the USM has with the larger time steps.

5.1 Integrator

All the simulations carried out require a reference trajectory, which cannot be determined analytically for perturbed orbits. Thus, a more accurate integration is used to first generate a so-called truth model. Both a fixed-step RK5 and a variable-step RK5(4) integrator is then used to find the error with respect to the truth model. For the variable-step method a more accurate integration can be obtained by either using a more stringent tolerance or by increasing the order of the integrator. For all the scenarios in this work, only the tolerances were made more stringent.

It is possible to derive all the various perturbations in terms of the USM (Altman 1972). However, usually users already have perturbations available in Cartesian form. By integration using the Cartesian form, we refer to Cowell's method, which is the integration of the following second order ODE:

$$\ddot{x} = -\mu \frac{x}{r^3} + a_{p_x}(t, x, y, z, \dot{x}, \dot{y}, \dot{z}) \tag{95}$$

$$\ddot{y} = -\mu \frac{y}{r^3} + a_{p_y}(t, x, y, z, \dot{x}, \dot{y}, \dot{z}) \tag{96}$$

$$\ddot{z} = -\mu \frac{z}{r^3} + a_{p_z}(t, x, y, z, \dot{x}, \dot{y}, \dot{z}) \tag{97}$$

where $r = \sqrt{x^2 + y^2 + z^2}$. Here, (x, y, z), $(\dot{x}, \dot{y}, \dot{z})$, $(\ddot{x}, \ddot{y}, \ddot{z})$, and $(a_{p_x}, a_{p_y}, a_{p_z})$ are the position, velocity, acceleration, and perturbing acceleration in the inertial frame.

To ensure that the USM can be easily implemented without much overhead and because the time required to switch between the USM and Cartesian coordinates is very small compared to the computation time required to compute the perturbations, perturbation models expressed in Cartesian coordinates have been used. The perturbations applied are: atmospheric drag, gravity up to degree and order 2, solar and lunar third-body perturbation, and solar-radiation pressure (SRP). These perturbations are the major sources of perturbation for Earth-orbiting satellites and the perturbation models can be easily found in literature. For the SRP perturbation, the simple cylindrical model was used (Montenbruck and Gill 2005). An exponential atmosphere for the Earth was implemented using look-up tables (Wertz and Larson 2003). The ephemeris for the Sun and Moon with respect to the Earth was computed from low-precision geocentric formulas (Van Flandern and Pukkinen 1979). The standard spherical harmonics equations for the Earth's gravity field are used (Montenbruck and Gill 2005). For the Mars orbiting scenario, an exponential atmosphere is implemented. If perturbations are to be used, the USM state is first converted to Cartesian coordinates prior to computing the perturbations. However, if only low-thrust propulsion is used, there is no need to convert the state to Cartesian coordinates since it is simpler to compute the perturbing accelerations in $\mathcal{F}_e$ than in $\mathcal{F}_g$.

When implementing the dynamics function for the USM, it is important to validate this with respect to both an unperturbed analytical and a perturbed numerical orbit, before they can be used to generate trajectories. For Cartesian coordinates the dynamics function is quite simple to implement and choosing an unperturbed, eccentric, and inclined orbit will sufficiently excite all the time derivatives. For the USM, however, an unperturbed orbit only causes a change in the quaternion. Unless a perturbed orbit is chosen, $\dot{C}$, $\dot{R}_{f1}$, $\dot{R}_{f2}$, and ω_1 will not be excited. Thus, any bug in the dynamics regarding those elements would not be found.

It is important to note that the tolerances are checked during the USM integration by converting the propagated state to Cartesian coordinates. This way, a consistent time step-size

adjuster is used for integration with both the USM and Cartesian coordinates. The variable step-size integrator requires two tolerance values ε_{pos} and ε_{vel}. After an integration step, both the actual 5th-order solution $\mathbf{y}$, and the embedded 4th-order solution $\mathbf{y}_{em}$ are used. If the integration is carried out using the USM, solutions are converted to Cartesian coordinates. The difference between the two vectors in Cartesian coordinates, Δ, is taken and then divided by the present time step-size h:

$$\Delta = \begin{bmatrix} \Delta\mathbf{r} \\ \Delta\mathbf{v} \end{bmatrix} = \frac{\mathbf{y} - \mathbf{y}_{em}}{h} \tag{98}$$

In case $|\Delta\mathbf{r}| \leq \varepsilon_{pos}$ and $|\Delta\mathbf{v}| \leq \varepsilon_{vel}$, the solution is accepted. Otherwise, the integration is repeated using a new time step-size h_{new}. Even if the solution is accepted, h_{new} is computed for the next integration step.

Two more values are defined to be

$$\delta r = S\left(\frac{\varepsilon_{pos}}{|\Delta\mathbf{r}|}\right)^{1/4} \tag{99a}$$

$$\delta v = S\left(\frac{\varepsilon_{vel}}{|\Delta\mathbf{v}|}\right)^{1/4} \tag{99b}$$

In Eq. (99) S is a safety factor, which is chosen to be 0.84. The difference δ to be used to find h_{new} is the smallest out of δr and δv.

$$h_{new} = \begin{cases} 0.1h & \text{if } \delta \leq 0.1, \\ \delta h & \text{if } 0.1 < \delta < 5, \\ 5h & \text{if } \delta \geq 5. \end{cases} \tag{100}$$

For each of the various USM methods, additional steps have to be taken after an integration solution is accepted:

USM7: If the norm of the quaternion is greater than 1, normalize the quaternion.
USM6: If the norm of the MRP vector is > 1, switch to SMRP and vice versa.
USMEM: If $\Phi > \pi$, switch between $\mathbf{a}$ and $\mathbf{a}^S$.

5.2 Perturbed orbits without thrust

A circular and an elliptic Molniya type of orbit with $e = 0.7$ are chosen as the reference orbits to be simulated. Trial runs using the USMEM showed that it has better integration performance and therefore, the truth-model is created using RK5(4) with Cash-Karp coefficients (Cash and Karp 1990) with the USMEM and $\varepsilon_{pos} = \varepsilon_{vel} = 10^{-8}$. The minimum and maximum time step-size were set to 5 s and 250 s, respectively. The initial Keplerian elements for the two orbits can be found in Table 1.

Table 1 Initial Keplerian elements of the reference orbits

Orbit type	a (km)	e (−)	i (deg)	Ω (deg)	ω (deg)	ν (deg)
Circular	6936	0.00	28.5	194.8	272.3	0.0
Elliptic	26559	0.70	63.2	206.3	281.6	0.0

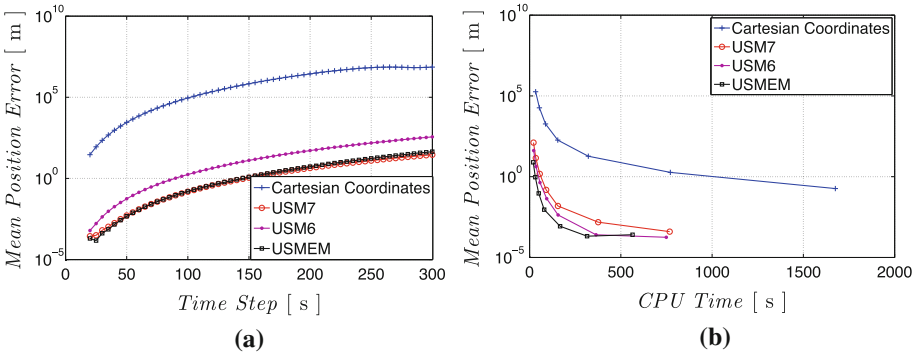

Fig. 3 Mean error in position against time step-size for 200 original orbital periods of a circular orbit (a) Fixed step (b) variable step

For the variable time-step, integration was again carried out using the RK5(4) with Cartesian coordinates and the USM for various tolerances. The position and velocity tolerances were set to the same value, $\varepsilon_{pos} = \varepsilon_{vel}$, and the tolerances were made more stringent by an order of magnitude for each simulation from 10^{-1} to 10^{-7}. The maximum and minimum time step-sizes were kept at 5 and 250 s respectively. For the fixed time-step, integration was carried out using RK5 with time step-sizes changed from 20 to 300 s with a jump of 5 s. The mean error in position between the truth-model and the simulated trajectory is computed for each simulation. This error is plotted against the CPU time for the variable time-step integration and against the time step-size for the fixed time-step integration. The mean error in velocity is not shown, because it follows the same trend as the position error and therefore does not provide any additional information. The CPU time was measured using the `tic toc` function available in MATLAB.

For the circular orbit case, the simulation was carried out for 200 original orbital periods. The mean position error for the fixed time-step integrations can be seen in Fig. 3a, whereas the one for the variable time-step integrations can be seen in Fig. 3b. Note that the mean error is a 3D RMS, which includes information on both the mean and deviation in a single value. Therefore, every variation is bound to be included. When the error in position increases monotonically, this error should contain all the information necessary to decide which integration technique is better.

For the circular orbit case, the performance of the USMs is clearly superior to the Cartesian model. When fixed-step integration is used, the mean position error using the Cartesian model is always approximately four orders of magnitude larger than the mean position error of the USM models. Between the USM, the behavior of the USM7 and the USMEM is very similar. USM7 has a larger error for the smaller time step-sizes while USMEM has a larger error for the larger step-sizes. The errors using the USM6 seem to be always larger than the USM7 and USMEM by an order of magnitude. It is more important to consider the variable-step integration for all the results in this paper, because this is the method that is normally used for orbit integration. Variable-step integration adapts to the dynamics and therefore highlights the holistic performance of the model.

During the variable step-size integration, the results of the Cartesian model form a front in the position error-CPU time space (as seen in Fig. 3b). Any USM result below or to the left of this front can be considered to perform better than the Cartesian results for this particular implementation. It is clear that all of the USM results are better than the Cartesian results. For

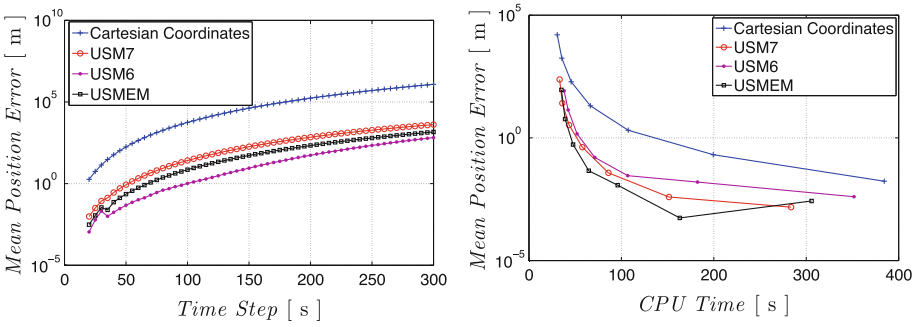

Fig. 4 Mean error in position against time step-size for 50 original orbital periods of a Molniya orbit (a) Fixed step (b) variable step

a given CPU time, integration using Cartesian coordinates has errors that are approximately 3–4 orders of magnitude larger than that of the USMs. Out of the various USM results, USMEM performs the best and the USM7 the worst. The error in USM6 is approximately half an order of magnitude more than that of the USMEM and the error in USM7 is approximately an order of magnitude larger than the USMEM for the same CPU time.

For the highly eccentric case, the simulation was carried for 50 original orbital periods. The mean position error for the fixed time-step integrations can be seen in Fig. 4a. The mean position error for the variable time-step integrations can be seen in Fig. 4b.

For the elliptical orbit case, the performance of the USMs is again superior to the Cartesian model. However, this difference is smaller than the difference found for the circular orbit. When fixed-step integration is used, the mean position error using the Cartesian model is always approximately two to three orders of magnitude larger than the mean position error of the USMs. This is because the error in the perigee passes is higher for Cartesian coordinates using the same time step-size as the USMs. However, the error in perigee passes results in larger overall error. Between the USMs, USMEM has an order of magnitude larger error than the USM6 and the USM7 has an order of magnitude larger error than the USMEM.

As can be seen in Fig. 4b, all of the USM results are better than the Cartesian results. Out of the various USMs, USMEM performs the best and the USM6 the worst. It can be seen that for this highly eccentric case, the error using Cartesian coordinates is only approximately two orders of magnitude larger than that of the USMs. For the less stringent tolerances, the difference between the different USMs is not very large. As the tolerance becomes more stringent (left side of Fig. 4b), USM6 has an order of magnitude larger error than USMEM and USM7 has half an order of magnitude larger error than the USMEM. When the error of USMEM gets in the range of 10^{-3} m, it can be assumed that the solution is converged and thus, there may be numerical jitter where the error seems to increase again.

This means that as the eccentricity become higher, there is less benefit of using the USMs. If the eccentricity is large enough, integration using the Cartesian coordinates can outperform the USMs as shown hereafter for the Mars aerobraking scenario.

5.3 Orbits using low-thrust propulsion

To test the performance of the USM for trajectories as a result of low-thrust propulsion, the following two thrusting scenarios have been used:

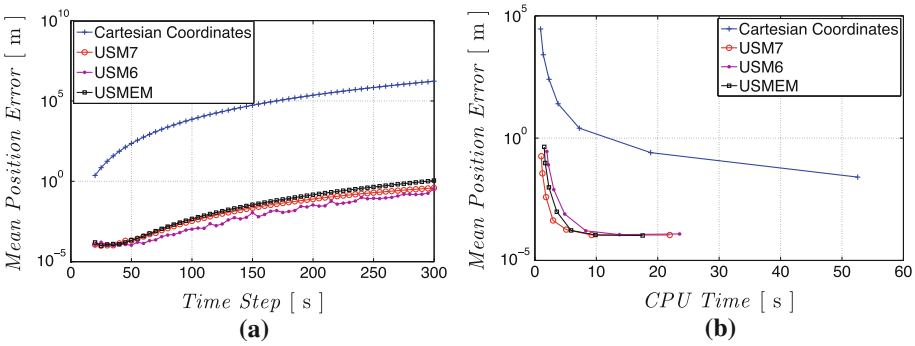

Fig. 5 Error in position for tangential low-thrust orbit (scenario 1) (a) Fixed step (b) variable step

Scenario 1 A circular parking orbit at an altitude of 838 km is used as the initial orbit and then simulated for 100 original orbit periods with a continuous tangential acceleration of 0.0005 g (0.004905 m/s^2). No other perturbing accelerations are used.

Scenario 2 A circular parking orbit at an altitude of 1000 km is used as the initial orbit. A continuous tangential acceleration of 0.001 g (0.00981m/s^2) is then applied till the spacecraft reaches GEO altitude. The spacecraft is under the influence of all perturbations and this trajectory is comparable to a low-thrust GTO.

All simulations were carried out with the same conditions for the integrators as for the orbits without thrust (Sect. 5.2).

For Scenario 1, no other perturbations were used so that the abilities of the USM to handle low-thrust orbits can be showcased. For this low-thrust case, no conversions have to be made to the Cartesian model to find the perturbations. The results of the fixed step-size integrator can be seen in Fig. 5a and of the variable step-size integrator can be seen in Fig. 5b.

The position error using a fixed step-size integrator is apparently for the USMs five to six orders of magnitude smaller than for the Cartesian model. For the variable step-size integrations, the position error for USM7, USMEM, and USM6 converge after a CPU time of approximately 9, 10 and 14 s, respectively. For integration using the Cartesian model, the error has not yet converged after a CPU time of approximately 53 s. Of the USMs, the USM7 performs the best, followed by USMEM and USM6.

In reality, low-thrust orbits also have perturbations. Thus, a full test of the USM should include a low-thrust orbit with perturbations as defined in Scenario 2. For this scenario the results of the fixed step-size integration can be seen in Fig. 6a and those of the variable step-size integration in Fig. 6b.

The results with low thrust and other perturbations are very similar to the results found for only low-thrust propulsion. Again, the USMs perform better than the Cartesian model. In this case, however, the performance of the USMEM is the best of the USMs, closely followed by USM6. USM7 is the worst of the USMs for both the fixed and the variable step-size integrations. During the fixed-step integration, there is a wobble-like behavior in the mean error for the USM6 and the USMEM. This only occurs when the error is lower than 10^{-2} m and is caused due to numerical jitter since the error is so low and the perturbations act in an erratic manner.

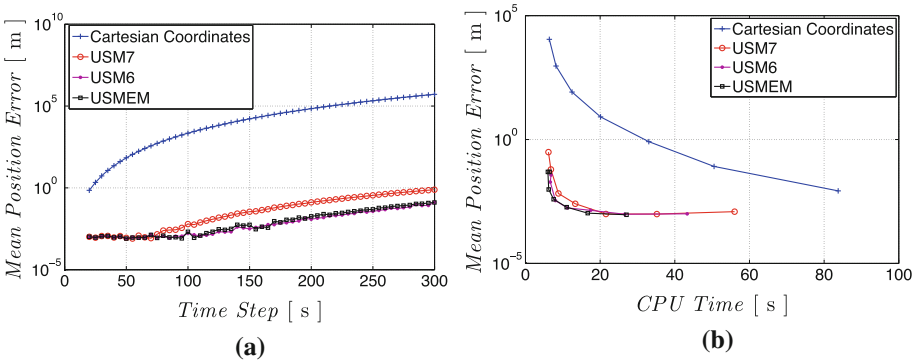

Fig. 6 Error in position for a low-thrust orbit raising maneuver with all perturbations (scenario 2) (a) Fixed step (b) variable step

Table 2 Initial Keplerian elements of the Martian orbit (Zhang et al. 2010)

a (km)	e (−)	i (deg)	Ω (deg)	ω (deg)	ν (deg)
31241	0.89	0.0	0.0	0.0	0.0

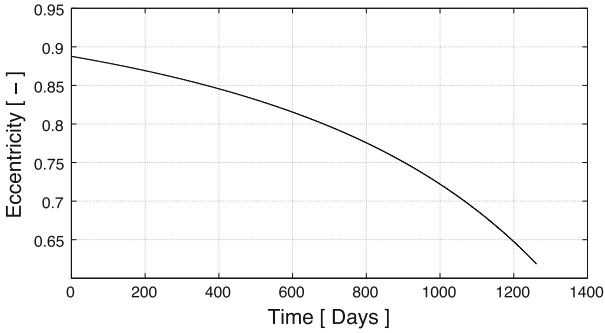

Fig. 7 Eccentricity as a function of time for an aerobraking maneuver around Mars (variable step-size integrator)

5.4 Mars aerobraking

The next set of simulations involve a satellite aerobraking in the Martian atmosphere. The initial conditions are those for a satellite at its periapsis in a highly eccentric orbit around Mars. The initial conditions for this orbit have been chosen similar to those of the Mars Reconnaissance Orbiter (MRO) and are given in Table 2. Only the variable step-size integrations are carried out for this case.

The evolution of the eccentricity can be seen in Fig. 7. The entire trajectory is flown in a highly eccentric orbit with eccentricity ranging from 0.89 to 0.62. Since this is a trajectory with a long mission duration, only the important results of the variable step-size integration are shown in Fig. 8.

This figure shows again that the USMs outperform Cartesian coordinates for this highly eccentric case. The error in the Cartesian coordinates is always almost an order of magnitude higher than the USMs. USMEM outperforms the other two USMs. This difference is minimal for less stringent tolerances but gets larger for higher accuracies. The difference between

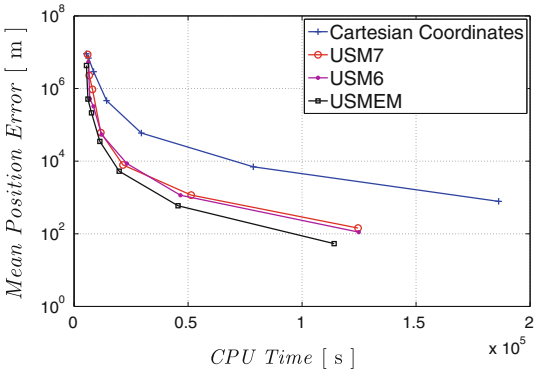

Fig. 8 Error in position for an aerobraking maneuver around Mars using a variable step-size integrator

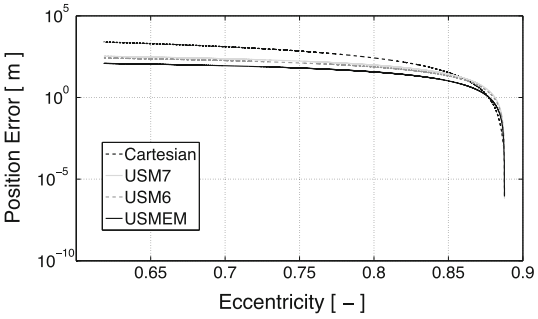

Fig. 9 Error in position as a function of eccentricity for an aerobraking maneuver around Mars using a variable step-size integrator

USM6 and USM7 is again minimal in the beginning, but the USM6 marginally outperforms the USM7 for the two most stringent tolerances.

The error in position as a function of the eccentricity of the osculating orbit can be seen in Fig. 9. This figure shows the development of the error throughout the simulation.

It can be seen that in the starting phases of the simulation, when the eccentricity is very high, Cartesian coordinates perform better than the USM. As the simulation proceeds, the error in Cartesian coordinates overtakes the USM error. This happens at an eccentricity of approximately 0.875 for the USMEM and at 0.86 for both the USM7 and the USM6. USMEM has half the error of the USM6 and USM7, and the USM6 has a marginally lower error than the USM7.

5.5 Absolute comparison with integration techniques in literature

A few simulations are carried out that check the performance of the USM for two test cases found in Bond and Allman (1996) to get the absolute performance with some of the more complicated integration techniques available in literature. It is to be expected that these techniques outperform the USM as they are based on more complex theories such as the Sundmann transformation and the Variation of Parameters (VOP). These theories are not as straightforward to implement as Cowell's method or the USM since their derivative equations are much more complex and also require iterations (Dallas and Rinderle 2000). However, they are extremely well suited for eccentric orbits.

The first case is the oblate Earth plus the Moon as a perturbing third body, and the reader is referred to Bond and Allman (1996) for all the details of the implementation. A satellite in a highly eccentric orbit ($e = 0.95$) is propagated for roughly 50 original revolutions (288.1

Table 3 Comparison of several methods for the oblate Earth plus Moon problem (Bond and Allman 1996)

Method	Benchmark	Sperling–Burdet	Kustaanheimo–Stiefel	Cowell
x [km]	−24219.050	−24218.818	−24219.002	-24182.152
y [km]	227962.106	227961.915	227962.429	227943.989
z [km]	129753.442	129753.343	129753.822	129744.270
Steps/rev	500	62	62	240
RSS error	–	0.318	0.501	42.5

Table 4 Comparison of several methods for the oblate Earth plus Moon problem using the USM

Method	Cartesian	USM7	USMRP	USMEM
x [km]	−24216.648	−24219.049	−24219.059	−24219.048
y [km]	227960.929	227962.106	227962.110	227962.105
z [km]	129752.846	129753.442	129753.445	129753.442
Steps/rev	436	372	386	384
RSS error	39.4	42.1	42.1	42.1

days) and the error at the end is compared to some standard integration techniques available in literature. All the results are tested against an accurate benchmark integration carried out in Stiefel and Scheifele (1971). Comparisons are also made to the Sperling–Burdet method found in Bond and Fraietta (1991), the Kustaanheimo–Stiefel method from Bond (1974), and the Cowell method from Bond and Hanssen (1973).

The results of the original comparison from Bond and Allman (1996) can be seen in Table 3. The results of using the USM models and Cartesian coordinates with the Cash-Karp integrator defined in Sect. 5.1 can be seen in Table 4. As expected, the more complex methods outperform the USM because the suitability of these methods for highly eccentric orbits. Even the Cartesian-coordinate method slightly outperforms the USM, which all behave in roughly the same way. This is also to be expected since Fig. 9 already showed that integration using Cartesian coordinates is much more suitable for highly eccentric orbits. Also, the comparisons made here are with function evaluations only and not with the CPU time. The more complex methods might actually require much more CPU time as each integration step might be very CPU intensive due to the complex derivative equations. Apart from being difficult to implement, these methods are also not very intuitive. This is not the case with the USM, where each of the state variables has a physical meaning like Cartesian coordinates and Keplerian elements.

The other example that is used here is the one with continuous radial thrust described in Batting (1999). A spacecraft is in a circular equatorial orbit at $r = 6800$ km and the radial thrust is applied till the spacecraft escapes. The results of USM methods using an RK4 fixed step-size integrator with a step-size of approximately 105 s are compared with the solution from the Sperling–Burdet approach and the analytical method, found in Bond and Allman (1996). The error in the position for the various methods can be seen in Table 5. Again, the Sperling–Burdet method has lower error than the USM. However, the USM outperforms integration using Cowell's technique as can be predicted from the results in Sect. 5.3.

These absolute comparisons have been shown in order to try to place the USM in the overall accuracy of the various integration methods available. The USM is not as accurate as

Table 5 Comparison of the USM methods with results from Bond and Allman (1996) for continuous radial thrust

Method	Time (s)	Position error (km)
Sperling–Burdet	12, 000	0.00013
Cartesian	12, 000	0.356
USM7	12, 000	0.013
USMRP	12, 000	0.014
USMEM	12, 000	0.015

the Sperling–Burdet or the Kustaanheimo–Stiefel approach. These advanced techniques are suggested for applications such as precise orbit determination, or long-term orbit simulation. However, for first-order mission-analysis applications where normally Cowell's method is used along with a Runge-Kutta integrator of arbitrary order, the USM techniques are comparable to Cartesian coordinates in terms of ease of implementation, but are superior in terms of performance.

5.6 Integration using high-degree spherical harmonics

So far, only low-degree gravitational perturbations have been considered during the propagation of several orbits. Once the order of the gravity field increases one cannot increase the step size indefinitely, because for too large step sizes higher harmonics of the gravity field may not be captured anymore. This is particularly true for orbits that are close to the Earth's surface. To study whether the step size as determined by the integrator is not too large for this kind of orbit, we will propagate the low circular orbit of Table 1 once more, but now with a much higher order and degree spherical harmonics model to define the gravitational perturbations (other perturbations are not considered). Since the orbital energy of a satellite in a conservative force field should be constant, we will be able to check the influence of the integration time step on the solution. The selected gravity field is the 70×70 ITG-Grace2010 gravity-field model (Mayer-Gürr et al. 2010). It is based on daily gravity solutions calculated using a Kalman smoother, unconstrained monthly solutions, and a high-resolution long-time mean.

It can be shown that the orbital-energy content of a satellite in a rotating potential field does not only consist of the kinetic and (static) potential energy, V, but also includes a centrifugal potential due to the rotation of the central body (Visser et al. 2003). The total specific energy E (*i.e.*, energy per unit mass) is in that case given by

$$E = \frac{1}{2}\mathbf{v_e} \cdot \mathbf{v_e} - \frac{1}{2}(\boldsymbol{\omega} \times \mathbf{r_e}) \cdot (\boldsymbol{\omega} \times \mathbf{r_e}) + V \tag{101}$$

where $\mathbf{r_e}$ and $\mathbf{v_e}$ are the position and velocity vector in the Earth-centred Earth-fixed frame, and $\boldsymbol{\omega}$ is the Earth's angular rotation rate.

Simulating the circular orbit for 200 orbital periods with each of the four state models gives the energy-error plot of Fig. 10. For the sake of clarity only a limited part of the time frame has been plotted; it is noted that the repeating pattern is constant for the full duration of the simulation. The maximum energy error for each of the USMs is around 10^{-7}%, and for the the Cartesian coordinates about 10% larger. The corresponding minimum error is around 10^{-11} and 10^{-8}, respectively. For practical purposes we can conclude that indeed the orbital energy remains constant for each of the state models. However, the number of function evaluations for the complete simulation duration is smallest for the USMEM (40,901), 5.7%

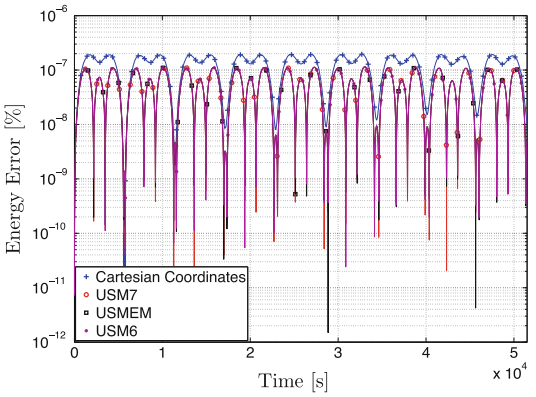

Fig. 10 Relative error in orbital energy for a satellite in a circular orbit (variable step-size integrator)

more for the USM6, 8.7% for the USM7 and 48.3% for the Cartesian coordinates. So, also for the high-order gravitational perturbations the USMs are the preferred state models. For a geostationary orbit, similar results are obtained, which leads to the assumption that the same also holds for any elliptical orbit in between these two orbit types.

6 Conclusions

The goal of this paper was to re-introduce the elegant, but apparently forgotten USM. The complete derivation of the original model was never provided in literature. Therefore, we have shown it here, so that the model might be better understood and then used by others in the field. The additional modifications show that any set of parameters that can hold attitude information can be used in conjunction with the USM.

It was found that all variations of the USM can be used for all the applications that the Cartesian coordinates are used for with very few adaptations. For unperturbed orbits, the behavior of the USM is excellent because the orbital energy and the angular momentum are conserved. The USM can also be used for parabolic and hyperbolic trajectories. Hyperbolic trajectories are well represented within the sphere of influence of planets and thus, the patched conic method can be used for the USM for interplanetary trajectories. Other than the singularity present for pure retrograde orbits, there are no other theoretical scenarios where the USM cannot be used. However, the true anomaly limit for hyperbolic orbits causes a practical limit due to the slow change in the true anomaly near this limit.

For perturbed orbits, the USM performs better than Cartesian coordinates for both fixed-step and variable-step integration. For very small time step sizes, the USM and Cartesian results are very similar. However, the error of the USM is much lower when larger time steps are used. This can also be seen in the results for the variable-step integration as the USM performs much better than the Cartesian model with smaller simulation times. Even though all the cases in this work have shown the USM to be better than Cartesian coordinates, it was shown that if orbits with eccentricities larger than approximately 0.86 have to be simulated, it is better to use the Cartesian coordinates. In which case, the satellite spends much more time in an almost linear trajectory. Integration in Cartesian coordinates is inherently better suited for this as each state advancement is linear. The best solution would be to have a hybrid method that uses Cartesian coordinates for the more straight sections of the orbit and the USM near the periapsis and apoapsis. For all other commonly used orbits, however, the

USM still performs better than Cartesian coordinates. For example, a GTO, with an eccentricity of around 0.7, still has more accurate results when the USM is used. The scenario where the USM truly shines is low-thrust propulsion. When the thrust is the only perturbing force, the USM has position errors that are four - five orders of magnitude lower than the Cartesian model, when using a variable step-size integrator.

As the USM outperforms Cartesian coordinates for low to moderate eccentricity and continuous thrust orbits, we highly recommend its usage in optimizers. For an optimization problem many different trajectories have to be simulated, which make the computation time very long. Thus, using the USM would help in reducing this CPU load. In particular, low-thrust trajectories with electric propulsion or solar sailing would be the optimal target group of the USM. Because of the stability, we also recommend the USM for long-term orbit simulation. The fact that the USM performs better for low-eccentricity orbits should not be a deterrent as orbits of most satellites and debris are circular. For very precise orbit computations, however, it is recommended to use more advanced techniques such as Sperling–Burdet or Kustaanheimo–Stiefel.

Between the different USM variations, we recommend the newly proposed USMEM to be used for numerical integration of orbits. It is outperformed by USM7 only in the case of low-thrust propulsion with constant acceleration and no perturbations. This is not a realistic scenario and it can also be handled by other analytical methods such as exponential sinusoids. The USM6 and USM7 perform similarly for most cases and therefore, neither of them has a clear advantage over the other. The dynamics of the quaternions are very fast to compute and the quaternions have no singularity. However, the unit norm constraint is often violated and this is detrimental to the quaternion performance. The MRP and EM both have singularities that can be effectively bypassed. Although, this involves a higher amount of bookkeeping, in the case of the EM this results in a definite payoff over quaternions.

References

Altman, S.P.: Orbital Hodograph Analysis. AAS science and technology series 3, North Hollywood Western Periodicals (1965)

Altman, S.P.: Acceleration hodograph analysis techniques for powered orbital trajectories. Nasa-cr-61616, NASA (1967a)

Altman, S.P.: Hodographic treatment of the restricted three body problem. Tech. Rep. NASA-CR-61615, NASA (1967b)

Altman, S.P.: A unified state model of orbital trajectory and attitude dynamics. Celest. Mech. **6**, 425–446 (1972)

Altman, S.P.: Velocity-space maps and transforms of tracking observations for orbital trajectory state analysis. Celest. Mech. **11**, 405–428 (1975)

Apostolatos, T.A.: Hodograph: a useful geometrical tool for solving some difficult problems in dynamics. Am. J. Phys. **71**(3), 261–266 (2003)

Batting, R.H.: An Introduction to the Mathematics and Methods of Astrodynamics, Revised Edition. AIAA Education Series, American Institute of Aeronautics and Astronautics, Inc. (1999)

Bond, V.R.: The uniform, regular differential equations of the KS transformed perturbed two-body problem. Celest. Mech. **10**, 303–318 (1974)

Bond, V.R., Allman, M.C.: Modern Astrodynamics: Fundamentals and Perturbation Methods. Princeton University Press, Princeton (1996)

Bond, V.R., Fraietta, M.F.: Elimination of secular terms from the differential equations for the elements of the perturbed two-body problem. In: Proceedings of the Flight Mechanics and Estimation Theory Symposium-1991, Greenbelt, Maryland. NASA/Goddard Space Flight Center (1991)

Bond, V.R., Hanssen, V.: The Burdet formulation of the perturbed two-body problem with total energy as an element. Tech. Rep. JSC Internal 73-FM-86 (JSC-08004), NASA/Johnson Space Center (JSC) (1973)
Breiter, S.: Explicit symplectic integrator for highly eccentric orbits. Celest. Mech. Dyn. Astron. **71**(4), 229–241 (1998)
Cash, J.R., Karp, A.H.: A variable order Runge-Kutta method for initial value problems with rapidly varying right-hand sides. ACM Trans. Math. Softw. **16**(3), 201–222 (1990)
Chodas, P.: Application of the extended Kalman filter to several formulations of orbit determination. UTIAS Technical Note 224, University of Toronto Institute for Aerospace Studies (1981)
Crassidis, J.L., Markley, F.L.: Sliding mode control using modified rodrigues parameters. J. Guidance Control Dyn. **19**(6), 1381–1383 (1996)
Dallas, S., Rinderle, E.A.: A comparison os Cowell's method and a variation-of-parameters method for the computation of precision satellite orbits. Technical Report 32-1526, JPL (2000)
Eades, J.B.: Orbit information derived from its hodograph. Tech. Rep. TM X-63301, NASA (1968)
Fukushima, T.: New two-body regularization. Astron. J. **133**(1), 1–10 (2007a)
Fukushima, T.: Numerical comparison of two-body regularizations. Astron. J. **133**(6), 2815–2824 (2007b)
Grassia, F.S.: Practical parameterization of rotations using the exponential map. J. Graph. Tools **3**, 29–48 (1998)
Hintz, G.R.: Survey of orbit element sets. J. Guidance Control Dyn. **31**(3), 785–790 (2008)
Hughes, P.C.: Spacecraft Attitude Dynamics. Wiley, New York (1986)
Jezewski, D.J.: A comparative study of Newtonian Kustaanheimo/Stiefel, and Sperling/Burdet optimal trajectories. Celest. Mech. **12**(3), 297–315 (1975)
Jizheng, C., Jianping, Y., Qun, F.: Flight vehicle attitude determination using the modified rodrigues parameters. Chin. J. Aeronaut. **21**(5), 433–440 (2008)
Kurcheeva, I.V.: Kustaanheimo–Stiefel regularization and nonclassical canonical transformations. Celest. Mech. **15**, 353–365 (1977)
Mayer-Gürr, T., Kurtenbach, E., Eicker, A.: ITG-Grace2010, http://www.igg.uni-bonn.de/apmg/index.php?id=itg-grace2010. Last accessed 15 April 2010 (2010)
Montenbruck, O., Gill, E.: Satellite Orbits: Models, Methods and Applications. Springer, Berlin (2005)
Pelaez, J., Hedo, J.M., Andres, P.R.de : A special perturbation method in orbital dynamics. Celest. Mech. Dyn. Astron. **97**(2), 131–150 (2007)
Petit, J.M.: Symplectic integrators: rotations and roundoff errors. Celest. Mech. Dyn. Astron. **70**, 1–21 (1998)
Petropoulos, A.E., Longuski, J.M.: Shape-based algorithm for automated design of low-thrust, gravity-assist trajectories. J. Spacecraft Rockets **41**(5), 787–790 (2004)
Raol, J.R., Sinha, N.K.: On the orbit determination problem. In: IEEE Transactions on Aerospace and Electronic Systems, IEEE, vol AES-21, pp. 274–291 (1985)
Schaub, H., Junkins, J.L.: Analytical Mechanics of Aerospace Systems. AIAA Education Series, AIAA (2002)
Silver, M.: A short derivation of the Sperling–Burdet equations. Celest. Mech. **11**, 39–41 (1975)
Stiefel, E.L., Scheifele, G.: Linear and Regular Celestial Mechanics. Springer, Berlin (1971)
Sun, F.: Hodograph analysis of the free-flight trajectories between two arbitrary terminal points. Contractor Report CR-153, NASA (1965)
Thompson, B.F., Choi, K.K., Piggott, S.W., Beaver, S.R.: Orbital targeting based on hodograph theory for improved rendezvous safety. J. Guidance Control Dyn. **33**(5), 1566–1576 (2010)
Tsitouras, C.: A tenth order symplectic Runge-Kutta-Nyström method. Celest. Mech. Dyn. Astron. **74**(4), 223–230 (1999)
Van Flandern, T.C., Pukkinen, K.F.: Low-precision formulae for planetary positions. Astrophys. J. Suppl. Ser. **41**, 391–411 (1979)
Visser, P., Sneew, N., Gerlach, C.: Energy integral method for gravity field determination from satellite orbit coordinates. J. Geodesy **77**, 207–216 (2003)
Vittaldev, V., Mooij, E., Naeije, M.C.: Performance aspects of orbit propagation using the unified state model. In: AIAA/AAS Astrodynamics Specialist Conference (2010)
Vivarelli, M.D.: The KS-transformation in hypercomplex form. Celest. Mech. **29**, 45–50 (1983)
Vivarelli, M.D.: The KS-transformation in hypercomplex form and quantization of the negative-energy orbit manifold of the kepler problem. Celest. Mech. **36**, 349–364 (1985)
Waldvogel, J.: Quaternions and the perturbed Kepler problem. Celest. Mech. Dyn. Astron. **95**, 201–212 (2006)
Wertz, J.R., Larson, W.J.: Space Mission Analysis and Design, 3rd edn. Microcosm Press and Kluwer Academic Publishers, Dordrecht (2003)
Yoshida, H.: A new derivation of the Kustaanheimo–Stiefel variables. Celest. Mech. **28**, 239–242 (1982)
Zhang, W., Han, B., Zhang, C.: Spacecraft aerodynamics and trajectory simulation during aerobraking. Appl. Math. Mech. Engl. Ed. **31**(9), 1063–1072 (2010)